# The Role of the Lipid Bilayer in Tau Aggregation

Shana Elbaum-Garfinkle,[†] Trudy Ramlall,[§] and Elizabeth Rhoades[†‡*]
[†]Department of Molecular Biophysics and Biochemistry, [‡]Department of Physics, Yale University, New Haven, Connecticut; and [§]Department of Biochemistry, Weill Medical College of Cornell University, New York, New York

ABSTRACT Tau is a microtubule associated protein whose aggregation is implicated in a number of neurodegenerative diseases. We investigate the mechanism by which anionic lipid vesicles induce aggregation of tau in vitro using K18, a fragment of tau corresponding to the four repeats of the microtubule binding domain. Our results show that aggregation occurs when the amount of K18 bound to the lipid bilayer exceeds a critical surface density. The ratio of protein/lipid at the critical aggregation concentration is pH-dependent, as is the binding affinity. At low pH, where the protein binds with high affinity, the critical surface density is independent both of total lipid concentration as well as the fraction of anionic lipid present in the bilayer. Furthermore, the aggregates consist of both protein and vesicles and bind the $\beta$-sheet specific dye, Thioflavin T, in the manner characteristic of pathological aggregates. Our results suggest that the lipid bilayer facilitates protein-protein interactions both by screening charges on the protein and by increasing the local protein concentration, resulting in rapid aggregation. Because anionic lipids are abundant in cellular membranes, these findings contribute to understanding tau-lipid bilayer interactions that may be relevant to disease pathology.

## INTRODUCTION

Neurofibrillary tangles (NFTs) composed primarily of the protein tau, are the hallmark of a number of neurodegenerative disorders, including Alzheimer's disease and the frontotemporal dementias. Although it is not clear what precise role NFTs and other proteinaceous aggregates play in the development of disease, the identification of point mutations in tau that result in hereditary tauopathies suggests a direct connection between tau misfunction and neurodegeneration (1–5).

Natively, tau is a microtubule-associated protein (6) that functions to stabilize microtubules and plays a major role in the establishment of normal neuronal morphology (7–13). Tau consists of two major segments: an N-terminal, or projection, domain that projects away from the microtubule surface, and a C-terminal region, which is responsible for microtubule binding and assembly (3,7,9,14). Within the C-terminal half of the protein are repeats of a highly conserved tubulin binding motif (15). In the adult brain, there are six isoforms of tau formed by alternative splicing that differ in the number of tubulin binding repeats (three or four) and the absence or presence of one or two inserts in the N-terminus (Fig. 1).

In solution, tau does not show any evidence of adopting stable secondary or tertiary structure (16). However, NMR studies of the microtubule binding domain have reported a propensity both for $\alpha$-helical (17) as well as $\beta$-sheet (18,19) structure in these regions. It has been hypothesized that this domain becomes at least partially structured on binding microtubules (20,21), although much of the N-terminus appears to remain disordered (11). The assumption of structure is also relevant to tau pathology, as conformational changes precede the formation of fibrillar aggregates (22,23) known as paired helical filaments, PHFs. PHFs, which further assemble to form NFTs, are rich in $\beta$-sheet structure.

Full length tau is highly soluble and does not aggregate over the course of many days under physiological concentrations and conditions in vitro. To catalyze aggregation reactions on reasonable experimental timescales, negatively charged molecules are typically used as aggregation inducers (24–26). Among the most common are polyanions such as heparin, RNA (25), and fatty acids (27–29). Anionic micelles, synthetic particles, and lipid vesicles have also been shown to induce tau fibrillization (22,26,30,31). Lipids are of particular interest as they are abundant in the cellular environment and accessible to cytosolic tau. Furthermore, there is evidence that fibrillar tau aggregates are associated with the cell membrane (32) and it has been suggested that interactions between tau and cell membranes may be relevant for its native function (33–36). Although the significance of the interactions between tau and lipid membranes has been shown, they are not well understood. Because binding of tau to lipid bilayers may have both functional and pathological manifestations, investigating the nature of this interaction is the focus of our current work.

In this study, we use K18, a fragment of tau that consists of all four microtubule binding repeats (Fig. 1) (8). Fragments of tau, such as K18, that span the microtubule-binding domain exhibit accelerated aggregation as compared to the full length protein (37). In addition, this domain forms the

*Submitted December 16, 2009, and accepted for publication March 2, 2010.*

*Correspondence: elizabeth.rhoades@yale.edu

*Abbreviations used:* AL488, Alexa Fluor 488; CAC, critical aggregation concentration; FCS, fluorescence correlation spectroscopy; LUVS, large unilamellar vesicles; NFT, neurofibrillary tangle; PC, 1-palmitoyl-2-oleoyl-*sn*-glycero-3-phosphocholine; PHFs, paired helical filaments; PS, 1-palmitoyl-2-oleoyl-*sn*-glycero-3-phospho-L-serine; ThT, thioflavin T; rhod-PE, 1,2-dioleoyl-*sn*-glycero-3-phosphoethanolamine-N-(lissamine rhodamine B sulfonyl).

Editor: William C. Wimley.


0006-3495/10/06/2722/9 $2.00

doi: 10.1016/j.bpj.2010.03.013

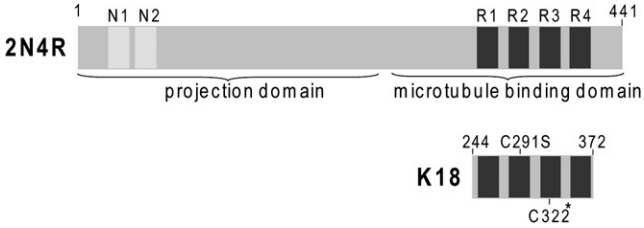


FIGURE 1 Tau constructs. The largest isoform (2N4R) is shown to illustrate relevant domains of the protein: the projection domain, with amino-terminal inserts, N1 and N2, and the microtubule binding domain with repeats R1–R4. Either or both N1 and N2, as well as R2, may be absent due to alternative splicing. Also shown is the fragment K18 (129 residues, containing R1–R4). $Cys^{322}$, which is used for site-specific fluorescent labeling, is marked with an asterisk (*). All numbering of residues in K18 is based on the 2N4R isoform.

core $\beta$-sheet region of PHFs (38), making fragments attractive models for the study of tau aggregation. We investigate both equilibrium binding of K18 to anionic lipid vesicles, as well as vesicle-induced aggregation of tau. Strikingly, we find that aggregation occurs at sub-$\mu$M protein concentrations when a critical concentration of tau bound to the lipid bilayer is exceeded, consistent with a nucleated aggregation mechanism. Furthermore, whereas aggregates are composed both of protein and vesicles, aggregation does not significantly disrupt the lipid bilayer. Our findings suggest that by screening charges and increasing the local protein concentration, the lipid bilayer serves to facilitate protein-protein interactions favorable for aggregation.

## MATERIALS AND METHODS

### Protein expression and purification

The DNA encoding K18 was cloned from the full length protein, 2N4R (Fig. 1), into a vector containing a cleavable His-tag to facilitate purification. Purification followed published protocols (39) with a few minor modifications (see Supporting Materials for details). After checking for purity by SDS-PAGE, the protein was lyophilized and stored at −20°C until use.

### Fluorescent labeling of proteins

Site-specific labeling of K18 was achieved using a maleimide-reactive fluorophore on a cysteine residue. K18 contains cysteines at positions 291 and 322 (Fig. 1). Cysteine 291 was mutated to a serine (C291S) using a QuickChange Site-Directed Mutagenesis kit (Stratagene, Cedar Creek, TX) to remove this potential labeling site to ensure that each protein was labeled with only a single fluorophore. For labeling, ~0.1 mg Alexa 488 maleimide (Invitrogen, Carlsbad, CA) was incubated with 250 $\mu$L of ~100 $\mu$M K18, at room temperature for several hours, then overnight at 4°C. The free dye was removed using two coupled GE HiTrap 5-mL desalting columns. To maximize the fraction of labeled protein, the protein was passed over Thiopropyl Sepharose 6B resin (GE Healthcare, Pittsburgh, PA) to separate labeled from unlabeled protein. The final protein concentration was determined by a modified Lowry assay (Bio-Rad, Hercules, CA), and the labeling efficiency calculated using the dye concentration measured by absorbance and the protein concentration measured by the assay. Throughout the manuscript, we refer to the C291S mutant as K18, and the labeled construct as K18-AL488. Although intermolecular disulfide bonds have been shown to accelerate the aggregation of tau, they are not necessary for aggregation (24). By EM, the fluorophore-labeled tau formed fibrillar aggregates that were indistinguishable from those formed by unlabeled tau (data not shown). Monitoring the emission intensity of K18-AL488 both in the absence and presence of vesicles showed that although there is a slight decrease in the quantum yield of the Alexa 488 on conjugation to the protein, there is no change in the quantum yield of K18-AL488 on binding to vesicles.

### Vesicles

LUVs were prepared from 1:1, 7:3, and 9:1 (molar ratio) PS and PC (Avanti Polar Lipids, Alabaster, AL). Stock solutions of the lipids were prepared in chloroform at concentrations of 10 mg/mL and stored at −20°C for up to six months. To prepare vesicles, the appropriate volumes of each lipid were mixed and the chloroform was evaporated under a gentle stream of nitrogen, followed by overnight dehydration under vacuum. Lipids were rehydrated in MOPS buffer (20 mM MOPS, 50 mM NaCl, pH adjusted with NaOH) and extruded 21 times through two stacked 100 nm pore-size membranes in a Lipofast extruder (Avestin, Ottawa, Canada). The final lipid concentration of the extruded vesicles was confirmed using a total phosphorus assay (40,41). For samples requiring fluorescently labeled vesicles, a small amount (~1:10,000 molar ratio) of fluorescently labeled lipid rhod-PE was incorporated into the chloroform mixtures before evaporation (LUV-rhod).

Concentrations of lipid are reported as either 'total' or 'accessible' lipid. In calculating accessible lipid concentrations, we assumed that the protein does not insert into the membrane so that it only has access to the outer leaflet of the bilayer. We estimated that for a ~100 nm diameter vesicle, ~10% more lipid resides in the outer leaflet than in the inner leaflet (42), and thus calculated accessible lipid concentrations based on measured total lipid concentrations from the phosphorous assay.

### FCS

FCS was measured in a lab-built instrument based on an inverted microscope that has been described previously (43,44). Generally, 20 autocorrelation curves were collected at each measurement condition and were analyzed using MATLAB (The MathWorks, Natick, MA) programs developed in the lab. All measurements were made at room temperature, which is maintained at 20.5 ± 0.11°C.

By measuring the diffusion times of fluorescent molecules, FCS can be used to study aggregation and binding of a species diffusing in solution. For aggregation assays, the amount of lipid was held fixed and protein was titrated into the vesicle solution. This assay was carried out in two formats: the first used fluorescently labeled protein and unlabeled vesicles and the second used unlabeled protein and fluorescently labeled vesicles. In both cases, aggregation is observed as an irreversible destabilization of the autocorrelation curve (see Fig. S1 for details). We use the term destabilization to emphasize that evidence of aggregation manifests itself heterogeneously but irreversibly (Fig. S1, *A* and *C* compared to *B* and *D*). A shift to the right indicating the presence of large fluorescence species is always observed, but the shape and amplitude of this curve varies greatly from experiment to experiment. Eventually the aggregated species settle out of solution, resulting in a complete loss of signal. Although aggregation was generally observed within the dead time of the experiment, for uniformity, autocorrelation curves were collected 20 min after addition of protein to a vesicle solution. This observation time was sufficient for the unambiguous differentiation of aggregation from the occasional spurious signal due to inhomogeneities in the vesicle solution, but still well before signal was lost due to precipitation of the aggregates.

For the aggregation experiments with fluorescently labeled vesicles, protein concentrations were tested in 50 nM increments, with each sample freshly prepared in a new sample chamber. The CAC was determined to be the first concentration at which destabilization of the autocorrelation curve occurs. The reported CAC value thus has a lower bound of uncertainty of 50 nM. For example, if the FCS signal is stable at 250 nM protein, but destabilized at 300 nM protein, the latter value was taken to be the CAC

when in fact the actual concentration could be anywhere between 250 nM and 300 nM.

For binding, the fluorescently labeled protein was held at a fixed concentration whereas the lipid concentration was increased by the addition of vesicles (45). The resulting autocorrelation curves were fit with the following equation:

$$G(\tau) = \frac{1}{N}\left[A\left(1+\frac{\tau}{\tau_{D1}}\right)^{-1}\left(1+\frac{\tau}{s^2\tau_{D1}}\right)^{-1/2} + q(1-A)\left(1+\frac{\tau}{\tau_{D}}\right)^{-1}\left(1+\frac{\tau}{s^2\tau_{D2}}\right)^{-1/2}\right]. \quad (1)$$

Where, $G(\tau)$ is the autocorrelation as a function of time $\tau$, $N$ is the total amount of protein added, $\tau_{D1}$ and $\tau_{D2}$ are the mean diffusion times of free protein and vesicle bound protein, respectively, $q$ is the ratio of vesicle fluorescence to monomer protein fluorescence, $A$ is the fraction of free protein, and $s$ is the ratio of the axial to radial dimensions of the observation volume (46). For our experiments, $N$ and $s$ are constants determined by the amount of protein present and the instrument optics, respectively. We also fix $\tau_{D1}$ and $\tau_{D2}$ to values determined by measurements of protein or vesicles alone, respectively, so that $A$ and $q$ are the only free parameters in the fit.

## Imaging of aggregates

Samples containing either LUV-rhod or unlabeled LUVs (50 $\mu$M total lipid) were incubated with 500 nM K18 for 20 min. Half the sample was removed and ThT was added to the remainder to a final concentration of 25 $\mu$M. An aliquot of each solution was placed in a sample chamber, and then visualized on the same microscope used for FCS. Images were taken in widefield mode with a fluorescent lamp for illumination and an EM-CCD camera (Andor Technology, Belfast, Ireland) set to a 0.2-s acquisition rate for detection. Filter sets were used to select for either ThT (ex 440/20, em 490/40; Chroma Technology) or rhodamine (ex 535/30, em 565lp; Chroma Technology) fluorescence. Control images were taken of samples in the absence of ThT and/or K18.

ThT binding was also measured by bulk fluorescence. Samples were prepared as above using unlabeled LUVs. After 20-min incubation the samples were transferred to cuvettes and ThT fluorescence was measured on a PTI Quantamaster C-61 fluorimeter (PTI, Birmingham, NJ), with 4-nm slit widths and excitation and emission wavelengths of 450 nm and 485 nm, respectively. Background samples consisted of 25 $\mu$M ThT and LUVs to quantify any interactions between ThT and the lipid bilayer as well as LUVs and K18 in the absence of ThT to determine whether scattering from the large aggregates affected the signal.

Control experiments using heparin (average MW, 3000 kDa; Sigma, St. Louis, MO) as an inducer were made for several K18 concentrations. For each of these experiments, the molar ratio of tau to heparin was a constant value, 4:1, and 50 $\mu$M ThT was present. Fluorimeter settings were as described above.

## RESULTS

With the aim of characterizing the interactions between tau and lipid bilayers, FCS was used as a sensitive measure of aggregation and binding. Initially, the interaction was monitored as increasing amounts of K18-AL488 were titrated into a fixed concentration of unlabeled LUVs. At pH 5, binding to vesicles was observed by an increase in the diffusion time of K18-AL488 from that of free protein (~450 $\mu$s) to that of the vesicles (~8 ms) (Fig. 2 *A*). With increasing protein concentrations, equilibrium binding was observed. Fits to the autocorrelation curves yield the diffusion time of the vesicles,

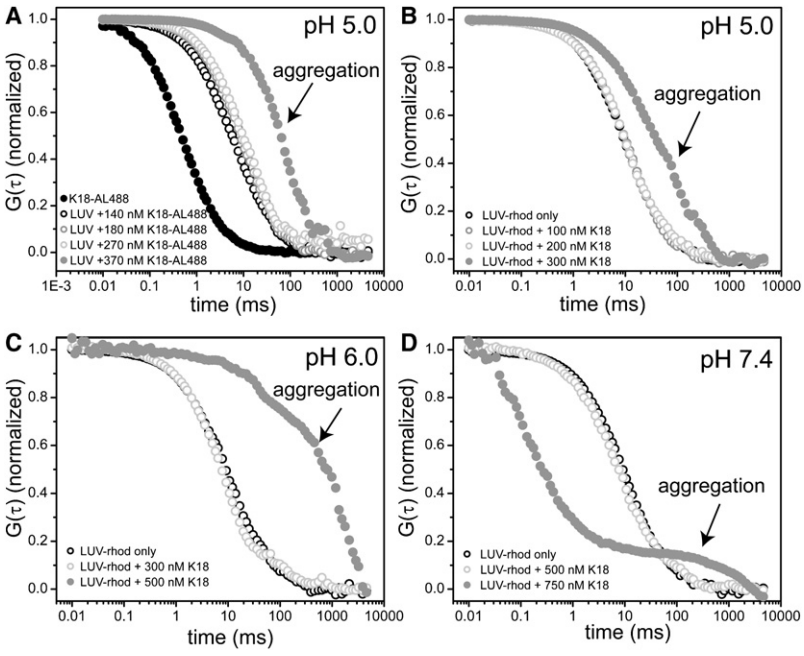


FIGURE 2 Aggregation of K18 by LUVs (50 $\mu$M lipid). (*A*) Autocorrelation curves of vesicle-induced aggregation of K18-AL488 at pH 5. For comparison, the autocorrelation curve of K18-AL488 in the absence of vesicles is shown (*solid black*). On addition of vesicles, the protein binds and the curves shift to longer times (*gray open*). Small shifts to the right are visible at higher protein concentrations may be due to an actual increase in the diffusion time of the vesicles when protein is bound, or simply normal variability in the vesicle sample. When the CAC is exceeded, the curves are destabilized—they shift markedly, unpredictably, and irreversibly to the right (*solid gray*). Longer incubation times result in complete disappearance of the autocorrelation signal, due to precipitation of the aggregated species. (*B*) Autocorrelation curves of vesicle-induced aggregation of K18 at pH 5. In contrast to *A*, K18 is unlabeled and the vesicles are fluorescently labeled (see Materials and Methods). The vesicle autocorrelation curves are unaffected by the presence of the protein (*open gray*) until the CAC is exceeded, at which time the curves shift markedly to the right (*solid gray*), analogous to the description in *A*. (*C* and *D*) Autocorrelation curves of vesicle-induced aggregation of K18 at pH 6 and pH 7.4, respectively, with labeled vesicles, as in *B*. The CAC increases with increasing pH. Comparing the aggregation curves shown in *B–D*, illustrates some of the variability in the observed autocorrelation curves on aggregation. The protein concentrations shown in *A–D* were chosen for illustrative purposes and represent only a subset of the concentrations measured for each condition.

with only a minor component due to unbound protein. Although equilibrium binding dictates that there will always be a small component of unbound protein, given that the lower bound of certainty in our measurements, as described in the Materials and Methods, is 50 nM, in these aggregation experiments, this amount of unbound protein should be significantly less than our measurement uncertainty and so we base our calculations on the assumption that the bound protein concentration is the total protein concentration. As the total protein concentration was further increased, the autocorrelation curves shifted markedly and unpredictably to the right, as described in the Materials and Methods and illustrated in Fig. S1. This shift is indicative of the presence of aggregated fluorescent species (Fig. 2 *A*). Notably, aggregation was observed with sub-$\mu$M K18 concentrations at pH 5, whereas for pH 6 and pH 7.4, aggregation was not observed for concentrations as high as several $\mu$M (data not shown). Although FCS measurements on our instrument become unreliable with >500 molecules/focal volume, aggregation in the form of destabilization of the autocorrelation curves would still be expected to be easily observable.

To monitor aggregation with an orthogonal probe, the experiments were repeated using fluorescently labeled vesicles (LUVs-rhod) and unlabeled protein. As with the first set of experiments, aggregation occurred on reaching a threshold protein concentration, the critical aggregation concentration (CAC). In contrast to the first set of experiments, aggregation was observed at sub-$\mu$M concentrations of K18 at all three pH values, with more protein required with increasing pH (Fig. 2, *B–D* and Table 1). Initially, stable autocorrelation curves with a diffusion time corresponding to that of the vesicles was observed, both in the absence of protein and with increasing protein concentrations. On reaching the CAC, destabilization of the autocorrelation curves indicative of aggregation occurred as observed in the previous experiment. Notably, the observation of large fluorescent species by FCS indicated that the vesicles were associated with the aggregated species. It is important to emphasize that below the CAC, aggregation was not observed even for significantly increased observation times. Below the CAC, vesicle and protein mixtures remained stable over the course of many hours (Fig. S2), whereas at the CAC, destabilization was evident within a few minutes. In the absence of vesicles, concentrations of K18 as high as 10 $\mu$M did not show any evidence of aggregation by either FCS or ThT fluorescence measurements at pH 5, 6, or 7.4 over the timescale of these experiments (data not shown).

To explain differences observed between K18-AL488 and unlabeled K18 at pH 6 and 7.4, we measured the affinity of K18-AL488 for the lipid bilayer by titrating unlabeled vesicles into a fixed concentration of labeled protein. For these experiments, ~20 nM protein was used to ensure that even at the lowest lipid concentrations, the protein/lipid ratio remained well below aggregation conditions as described above. We found that at pH 5 K18-AL488 binds to the vesicles with an apparent affinity, $K$, (in terms of lipid concentration) in the low $\mu$M, whereas at pH 6 and 7.4, the apparent $K$ is shifted over three orders of magnitude to the mM range (Fig. 3). Although the binding affinity may be expected to change with pH due to titration of groups both on the protein and on the lipids, such a dramatic shift suggests that at higher pH the interaction between the protein and the lipid bilayer is perturbed, most likely by the presence of the fluorophore on the protein that carries a charge of −2 at all pHs measured. The agreement between the results obtained for aggregation experiments on K18-AL488 and unlabeled K18 at pH 5 indicated that for this higher affinity interaction the presence of the fluorophore had significantly less of an effect.

To assess what factors, in addition to pH, influence the CAC, we repeated the experiments at pH 5 using different lipids concentrations and different ratios of PS/PC. The lipid to protein ratio at the CAC was found to be independent of the total amount of lipid present (Table 1, bold values in column 5), suggesting that the local concentration of protein at the vesicle surface was an important factor in initiating aggregation. Interestingly, increasing the relative amount of PS to PC from 1:1 to 7:3, and 9:1, had little effect on the measured CAC, ~250 nM protein for 50 $\mu$M total lipid (data not shown), despite the significant increase in binding affinity with increasing PS ratio (Fig. 3). From our experiments with labeled protein, we know that the majority of the protein is bound to the vesicles at the CAC (Fig. 2 *A*),

**TABLE 1 Comparison of the electrostatic properties and binding density of K18 and 1:1 PS/PC LUVs as a function of pH at the CAC**

| pH | $L_{acc}$ ($\mu$M) | K18 (nM) at CAC | K18/LUV | $L_{acc}$/K18 at CAC | Charge $L_{acc}$ ($\mu$M) | Charge K18 ($\mu$M) at CAC |
|---|---|---|---|---|---|---|
| 7.4 | 26.2 | 725 ±35 | 1340 | 36 | −13.1 | 7.5 |
| 6.0 | 26.2 | 375 ± 35 | 693 | 70 | −9.8 | 5.3 |
| 5.0 | 26.2 | 267 ± 33 | 493 | **98** | −3.3 | 4.4 |
| 5.0 | 52.4 | 533 ± 88 | | **98** | | |
| 5.0 | 104.8 | 1250 ± 25 | | **84** | | |

$L_{acc}$ is the accessible lipid concentration, calculated as described in the Materials and Methods. In determining the number of K18 molecules per vesicle, (K18/LUV), we calculated the number of vesicles using the known lipid concentration and assuming an average vesicle diameter of 100 nm and the average surface area of the lipid headgroup to be 68 Å$^2$ resulting in 92,400 lipids per vesicle. The bold numbers in column 5 from this calculation illustrate that the protein/lipid ratio at the CAC are within experimental error for several lipid concentrations. The average value of the three pH 5.0 measurements was used in the calculation of protein density at the CAC described in the Discussion, $L_{acc}$/K18 = 93. The charge concentration for accessible lipid (charge $L_{acc}$) assumes the charge per PS to be pH 7.4 = −1, pH6 = −0.75, and pH 5 = −0.25. Although rhod-PE is expected to carry a charge of +1 across the range of pHs used here, because it is used in very small amounts (1:10,000 molar ratio) relative to the other lipids, we do not take it into account in our calculations. The charge on K18 was calculated using Protein Calculator V3.3 (http://www.scripps.edu/~cdputnam/protcalc.html) and EMBOSS (http://emboss.bioinformatics.nl/cgi-bin/emboss/iep) programs: pH 7.4 = 10.3, pH 6 = 14.0, and pH 5 = 16.5. The shaded columns compare the total charge on the vesicles and on the protein at the CAC in units of concentration.

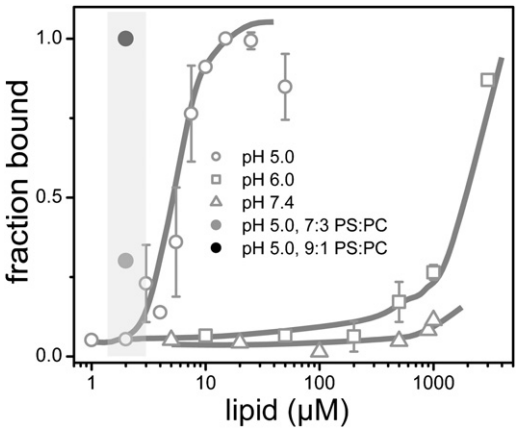


FIGURE 3 Binding of K18-AL488 to 1:1 PS/PC LUVs as a function of pH. Below the CAC, K18 binds vesicles without aggregating. The large shift in the apparent affinity between pH 5 (*open circles*) and pH 6 and 7.4 (*open squares* and *triangles*, respectively), suggests that at higher pH, the presence of fluorescent label may interfere with binding. Most points on the binding curves are the average of three independent measurements and the error bars are the standard error of these measurements. There are a few points obtained from single measurements that are also included in the curves; these points do not have any error bars associated with them. Lines are drawn to guide the eye. For comparison, the fraction K18 bound to vesicles composed of 7:3 (*gray solid circle*) and 9:1 (*black solid circle*) ratios of PS/PC for 2 $\mu$M total lipid are plotted (*gray shading* on plot). The amount of protein bound increases with the fraction of PS in the lipid bilayer.

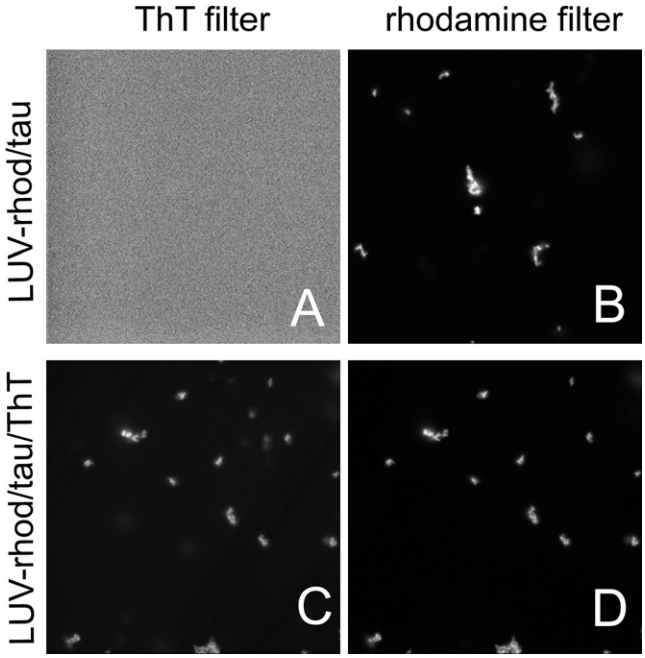


FIGURE 4 Images of aggregates formed by K18 and LUVs. (*A* and *B*) Samples imaged in the absence of ThT only show the presence of aggregates when the rhodamine filter set is used, evidence that there is no excitation of the rhodamine fluorophore with the ThT filter set. The image shows aggregates composed of LUV-rhod that are as large as several microns. (*C* and *D*) When 25 $\mu$M ThT is added to the samples before imaging, ThT positive aggregates colocalize with the LUV-rhod aggregates indicating that the K18 is associated with the aggregated lipids and capable of binding ThT in the characteristic manner associated with pathological aggregates.

suggesting that the surface density of protein on aggregation is the same for all three vesicle compositions. We thus conclude that although increasing the fraction of anionic lipid increases the binding affinity of K18 for the vesicles, the protein density on the vesicle surface at the CAC is unaffected by the increase in anionic charge of the vesicle.

To probe the structure of K18 in the aggregates, images of aggregated K18/LUV-rhod samples were taken with and without ThT (Fig. 4). In the absence of ThT, aggregated LUVs-rhod were visible (Fig. 4, *A* and *B*) as expected from the FCS measurements that indicated that the vesicles were incorporated into the aggregated species. On addition of ThT, the aggregates observed with the ThT filter set colocalized with those seen using the rhodamine filter set (Fig. 4, *C* and *D*), suggesting that the associated protein was capable of binding ThT in a manner characteristic of PHFs. In the absence of K18, there was no evidence of aggregated species in the samples (Fig. S3, *A* and *B*). Measurements of ThT fluorescence in a fluorimeter show that ThT does not interact strongly with the vesicles alone and that K18/vesicle aggregates give rise to a ThT signal above the background (Fig. S3 *E*). As a control, heparin induced aggregation of K18 was measured at 500 nM, comparable to concentrations used in our FCS experiments (Fig. S3 *F*). The ThT signal over the course of 1 h was only slightly greater than background.

Finally, leakage assays based on an encapsulated dye and quencher were used to test if tau aggregation compromised lipid bilayer integrity (see Supporting Materials for details). Under conditions where aggregation is readily observable by FCS for K18 (Fig. 2, *A* and *B*)—pH 5, 50 $\mu$M lipid, and 500 nM protein—no increase in fluorescence signal was observed (Fig. S4), indicating that the lipid bilayer remained intact.

## DISCUSSION

Tau is a microtubule binding protein that has been shown to interact with cellular membranes in vivo (33–36). We therefore sought to assess the capacity of tau to interact with lipid bilayers under conditions of physiological and pathological relevance. The primary results of our experiments are: i), vesicle induced aggregation of tau is pH dependent and occurs when a critical concentration of protein is bound to a vesicle; ii), the aggregate formed is composed of both protein and vesicles and binds ThT in a characteristic manner; and iii), the lipid bilayer integrity is not affected by aggregation. Below, we interpret our results by considering several properties of tau that are influenced by its interactions with lipid vesicles.

### Aggregated species

The data presented in this study shows that anionic vesicles are potent inducers of tau aggregation. Notably, aggregation

occurs rapidly on reaching a CAC (Table 1), consistent with the nucleated aggregation mechanism that has been proposed for tau (23,47,48). At pH 5, where we can use fluorescently labeled tau to determine that most of the total protein in solution is bound to the vesicles (Fig. 2 *A*), the CAC can be translated directly to a critical surface density. However, at pH 6 and 7.4, where the fluorescent probe seems to interfere with vesicle binding, we do not have a direct probe of amount of protein bound and thus can only monitor the total amount of protein present when aggregation is observed.

FCS has been used by a number of groups, including our own, to study stable binding interactions between proteins and peptides and vesicles (45,49,50,52,53), although to our knowledge, this is the first time it has been used to study the role of vesicle interactions in amyloid formation. In contrast to ThT fluorescence, FCS serves as a direct probe of the interaction between tau and its inducer. Moreover, because the vesicles are large particles relative to the protein, a signal is observable by FCS under conditions where protein aggregation is difficult to observe by ThT binding alone, notably at the sub-$\mu$M protein concentrations used in this study (Fig. S3, *E* and *F*). FCS shows that the aggregates are composed both of vesicles and protein (Fig. 2) and imaging of the aggregated species in the presence of ThT (Fig. 4 and Fig. S3) shows aggregated species bind ThT. ThT binding is associated with the presence of $\beta$-sheet structure in PHFs, as well as in prefibrillar intermediates (22,23). Our findings support an earlier study at much higher protein concentrations that found that vesicle induced aggregation of tau resulted in aggregates that were morphologically similar to PHFs formed under other conditions (30).

## Electrostatics

Anionic vesicles cause K18 to aggregate at very low ($<1$ $\mu$M) protein concentrations, requiring additional protein with increasing pH (Table 1). K18 contains a number of histidines that are expected to be neutral at physiological pH but positively charged at pH 5, raising the net positive charge of the protein with decreasing pH, and thereby increasing its affinity for anionic vesicles. However, lowering the pH also has the effect of decreasing the negative charge of vesicles by titrating a carboxyl group on the PS headgroup, an effect that should serve to reduce the attraction of positively charged K18 for the vesicles. Although determining the charge at a bilayer surface depends on numerous factors, including the ionic strength of the buffer and the mole fraction of PS present (54), these factors are invariant over our measurement conditions using 1:1 PS/PC vesicles. Because our analysis below is dependent on orders of magnitude calculations of liposome charge, our findings are not markedly altered by small shifts to the values used in our calculations (see Table 1).

Based on our measurements using labeled vesicles and unlabeled K18, we calculated overall charge of the protein and the lipids at the CAC of tau to determine the number of lipids per protein binding site (see Table 1 caption). Table 1 shows that at the CAC, the absolute value of the protein charge and the accessible charge on the vesicles are of the same order of magnitude, although the vesicle charge is of a greater absolute value than the K18 charge at pH 6 and 7.4, such that there is always sufficient negative charge to neutralize the positively charged proteins, whereas at pH 5, the absolute charge on the protein and accessible lipid are almost identical (shaded columns in Table 1). This suggests that charge neutralization plays a role in the vesicle-induced aggregation of K18. Negatively charged molecules used are commonly for in vitro studies of tau aggregation, and it is generally thought they function as inducers by neutralizing the positive charges of the MT binding domain (22,30). Lending support to this hypothesis is the observation that induced tau aggregation is generally pH dependent (55,56) and it has been suggested that a change in pH modulates the affinity of tau for its inducer (24). Our pH data, which shows that with increasing pH there is both a reduced binding affinity and as well as an increase in the amount of protein required for aggregation to occur (Fig. 2, *B–D*), qualitatively support this explanation. However, we also find that although K18 binds with an increased affinity to vesicles containing a larger fraction of anionic lipids, the CAC is independent of the total fraction of anionic lipid over the range we tested (Fig. 3). Along with the differences we observe in binding and aggregation at different pHs, this suggests that electrostatic shielding is not the only relevant factor.

## Surfaces

In addition to its role in mediating electrostatic interactions between tau proteins, the lipid bilayer also provides a surface that may facilitate protein-protein associations by increasing their local concentration. In their studies of fatty acid induced aggregation of tau, Chirita et al. (30) found that fatty acids were in micellar form when capable of promoting aggregation and proposed that the general induction mechanism for anionic micelles is by concentrating tau at their surface. Although heparin is not known to form micelles, it is a polymer and it has been proposed that a single heparin can coordinate several tau molecules, resulting in a local region of high protein concentration (57).

Because the majority of our data is at pH 5, we will consider this data for further calculations. At the CAC, there are ~93 accessible lipids per protein (determined as described in Table 1) independent of total protein and lipid concentration. To calculate the maximum area that a single protein could occupy on the lipid bilayer, we model K18 binding as a random coil. By FCS measurements of the diffusion time of K18-AL488 in solution, we calculate a hydrodynamic radius of ~36 Å, which is in reasonable agreement both with what is predicted for a highly denatured protein (58) as well as with published values of the radius of gyration

of K18 (59). The corresponding area on the bilayer occupied by random coil K18 is ~4100 Å$^2$. Using the value of 68 Å$^2$ for the area of a lipid headgroup in a fluid bilayer (42), the resulting number of lipids in one leaflet of the bilayer needed to accommodate a single K18 molecule is ~60. Because it is known that tau becomes partially helical on binding to lipid vesicles (21), thereby reducing its bilayer footprint, we can reasonably assume that the actual number of lipids required for binding is <60. Our measured value of 93 lipids is ~1.5 times greater than this maximum value, indicating that aggregation is unlikely to be triggered by relatively close packing of the protein on the bilayer surface. This modeling does not consider the case where tau may actually insert into the bilayer, but given that our leakage measurements do not indicate significant perturbation of the bilayer on aggregation (Fig. S4) and that polystyrene microspheres, which are impermeable to protein insertion, are also capable of promoting tau aggregation (23), this assumption is likely justified.

At pH 5, where essentially all the protein is bound before aggregation (Fig. 2 *A*), the CAC can be directly translated to a surface density. Assuming that a single vesicle (diameter = 100 nm) has a surface area ~31,400 nm$^2$, and that the protein bound to the vesicle is localized to the surface in a layer that is the thickness of an $\alpha$-helix (5 Å) plus a hydration layer (5 Å), the volume at the vesicle surface is ~31,400 nm$^3$/vesicle or $3.14 \times 10^{-20}$ L/vesicle. The number of proteins bound per vesicle at the CAC is ~493 (Table 1) or ~$8.19 \times 10^{-22}$ moles protein/vesicle. Thus the concentration of protein at the vesicle surface is ~26 mM, or almost five orders of magnitude greater than the bulk solution concentration. Even assuming a hydration layer 10 times as thick (50 Å) yields a surface concentration ~5 mM. This calculation illustrates how effectively the vesicle raises the local protein concentration at the bilayer interface. In a cellular context, such a mechanism may explain how normal physiological concentrations of tau may be induced to aggregate.

### Physiological role for lipids in aggregation

There is significant evidence, both in vitro and in vivo, that interactions between tau and the lipid bilayer may be of importance. EM images of vesicle induced tau aggregates found that a fraction of the filaments were associated with a vesicle at the terminus of the fiber (30). It has been suggested that PHF assembly in the cell may begin at the plasma membrane (34,60) and lipids have been found in the paired helical filaments purified from brains of Alzheimer's patients (61). Interactions with cellular membranes may also be relevant to the normal function of tau. It has also been proposed that one of the major roles of the N-terminal projection domain may be to mediate interactions with specific components in the cellular membrane (33,62,63). More relevant to our study is evidence that the microtubule binding repeats themselves may bind nonspecifically to lipid surfaces in the cell (64,65). Whereas our studies used vesicles composed of at least 50% PS, which is significantly higher than the estimated <20% PS found in plasma membranes (66) increased levels of PS are found in neural membranes of patients with Alzheimer's disease (67), and in vitro studies have shown that PS vesicles can effectively compete with microtubules for binding to tau (65).

## CONCLUSIONS

Our results show that anionic lipid vesicles are extremely effective at promoting aggregation of the microtubule binding domain of tau, and are capable of inducing aggregation at sub-$\mu$M protein concentrations. Moreover, the aggregated species formed consist of both protein and intact lipid vesicles. We propose that the mechanism of induction of aggregation of tau by lipid vesicles occurs through a combination of charge neutralization and providing a platform for favorable protein-protein interactions.

## SUPPORTING MATERIAL

Four figures and details of protein purification are available at http://www.biophysj.org/biophysj/supplemental/S0006-3495(10)00343-7.

The authors thank Professors A. Miranker and T. Baumgart and Drs. A. Nath and E. Sevcsik for insightful discussions, critical reading of and comments on the manuscript. We thank Professor L. Binder for the gift of the 2N4R plasmid and Professor L. Regan for use of her fluorimeter.

This work was supported by the National Science Foundation (grant 0919853) and National Institutes of Health (grant 5T32GM007223-35 to S.E.).

## REFERENCES

1. Lee, V. M., M. Goedert, and J. Q. Trojanowski. 2001. Neurodegenerative tauopathies. *Annu. Rev. Neurosci.* 24:1121–1159.
2. Ballatore, C., V. M. Lee, and J. Q. Trojanowski. 2007. Tau-mediated neurodegeneration in Alzheimer's disease and related disorders. *Nat. Rev. Neurosci.* 8:663–672.
3. Buée, L., T. Bussière, …, P. R. Hof. 2000. Tau protein isoforms, phosphorylation and role in neurodegenerative disorders. *Brain Res. Brain Res. Rev.* 33:95–130.
4. Goedert, M., and M. G. Spillantini. 2006. A century of Alzheimer's disease. *Science.* 314:777–781.
5. Garcia, M. L., and D. W. Cleveland. 2001. Going new places using an old MAP: tau, microtubules and human neurodegenerative disease. *Curr. Opin. Cell Biol.* 13:41–48.
6. Ahn, J. S., M. L. Radhakrishnan, …, K. S. Kosik. 2005. Defining Cdk5 ligand chemical space with small molecule inhibitors of tau phosphorylation. *Chem. Biol.* 12:811–823.
7. Brandt, R., and G. Lee. 1993. Functional organization of microtubule-associated protein tau. Identification of regions which affect microtubule growth, nucleation, and bundle formation in vitro. *J. Biol. Chem.* 268:3414–3419.
8. Gustke, N., B. Trinczek, …, E. Mandelkow. 1994. Domains of tau protein and interactions with microtubules. *Biochemistry.* 33:9511–9522.
9. Mandelkow, E. M., J. Biernat, …, E. Mandelkow. 1995. Tau domains, phosphorylation, and interactions with microtubules. *Neurobiol. Aging.* 16:355–362, discussion 362–363.

10. Samsonov, A., J. Z. Yu, …, S. V. Popov. 2004. Tau interaction with microtubules in vivo. *J. Cell Sci.* 117:6129–6141.
11. Santarella, R. A., G. Skiniotis, …, A. Hoenger. 2004. Surface-decoration of microtubules by human tau. *J. Mol. Biol.* 339:539–553.
12. Drechsel, D. N., A. A. Hyman, …, M. W. Kirschner. 1992. Modulation of the dynamic instability of tubulin assembly by the microtubule-associated protein tau. *Mol. Biol. Cell.* 3:1141–1154.
13. Ebneth, A., R. Godemann, …, E. Mandelkow. 1998. Overexpression of tau protein inhibits kinesin-dependent trafficking of vesicles, mitochondria, and endoplasmic reticulum: implications for Alzheimer's disease. *J. Cell Biol.* 143:777–794.
14. Cleveland, D. W., S. Y. Hwo, and M. W. Kirschner. 1977. Purification of tau, a microtubule-associated protein that induces assembly of microtubules from purified tubulin. *J. Mol. Biol.* 116:207–225.
15. Lee, G., R. L. Neve, and K. S. Kosik. 1989. The microtubule binding domain of tau protein. *Neuron.* 2:1615–1624.
16. Cleveland, D. W., S. Y. Hwo, and M. W. Kirschner. 1977. Physical and chemical properties of purified tau factor and the role of tau in microtubule assembly. *J. Mol. Biol.* 116:227–247.
17. Eliezer, D., P. Barré, …, L. Heend. 2005. Residual structure in the repeat domain of tau: echoes of microtubule binding and paired helical filament formation. *Biochemistry.* 44:1026–1036.
18. Cho, M. K., H. Y. Kim, …, M. Zweckstetter. 2007. Amino acid bulkiness defines the local conformations and dynamics of natively unfolded alpha-synuclein and tau. *J. Am. Chem. Soc.* 129:3032–3033.
19. Mukrasch, M. D., J. Biernat, …, M. Zweckstetter. 2005. Sites of tau important for aggregation populate beta-structure and bind to microtubules and polyanions. *J. Biol. Chem.* 280:24978–24986.
20. Butner, K. A., and M. W. Kirschner. 1991. Tau protein binds to microtubules through a flexible array of distributed weak sites. *J. Cell Biol.* 115:717–730.
21. Barré, P., and D. Eliezer. 2006. Folding of the repeat domain of tau upon binding to lipid surfaces. *J. Mol. Biol.* 362:312–326.
22. Chirita, C. N., E. E. Congdon, …, J. Kuret. 2005. Triggers of full-length tau aggregation: a role for partially folded intermediates. *Biochemistry.* 44:5862–5872.
23. Chirita, C. N., and J. Kuret. 2004. Evidence for an intermediate in tau filament formation. *Biochemistry.* 43:1704–1714.
24. Friedhoff, P., A. Schneider, …, E. Mandelkow. 1998. Rapid assembly of Alzheimer-like paired helical filaments from microtubule-associated protein tau monitored by fluorescence in solution. *Biochemistry.* 37:10223–10230.
25. Kampers, T., P. Friedhoff, …, E. Mandelkow. 1996. RNA stimulates aggregation of microtubule-associated protein tau into Alzheimer-like paired helical filaments. *FEBS Lett.* 399:344–349.
26. Kuret, J., E. E. Congdon, …, Q. Zhong. 2005. Evaluating triggers and enhancers of tau fibrillization. *Microsc. Res. Tech.* 67:141–155.
27. Barghorn, S., and E. Mandelkow. 2002. Toward a unified scheme for the aggregation of tau into Alzheimer paired helical filaments. *Biochemistry.* 41:14885–14896.
28. Wilson, D. M., and L. I. Binder. 1997. Free fatty acids stimulate the polymerization of tau and amyloid beta peptides. In vitro evidence for a common effector of pathogenesis in Alzheimer's disease. *Am. J. Pathol.* 150:2181–2195.
29. King, M. E., V. Ahuja, …, J. Kuret. 1999. Ligand-dependent tau filament formation: implications for Alzheimer's disease progression. *Biochemistry.* 38:14851–14859.
30. Chirita, C. N., M. Necula, and J. Kuret. 2003. Anionic micelles and vesicles induce tau fibrillization in vitro. *J. Biol. Chem.* 278:25644–25650.
31. Zhao, H. X., E. K. J. Tuominen, and P. K. J. Kinnunen. 2004. Formation of amyloid fibers triggered by phosphatidylserine-containing membranes. *Biochemistry.* 43:10302–10307.
32. Gray, E. G., M. Paula-Barbosa, and A. Roher. 1987. Alzheimer's disease: paired helical filaments and cytomembranes. *Neuropathol. Appl. Neurobiol.* 13:91–110.
33. Brandt, R., J. Léger, and G. Lee. 1995. Interaction of tau with the neural plasma membrane mediated by tau's amino-terminal projection domain. *J. Cell Biol.* 131:1327–1340.
34. Lira-De Leon, K. I., M. A. De Anda-Hernandez, …, M. A. Meraz-Rios. 2009. Plasma membrane-associated PHF-core could be the trigger for tau aggregation in Alzheimer's disease. *In* Current Hypotheses and Research Milestones in Alzheimer's Disease. Springer, New York, NY.
35. Maas, T., J. Eidenmüller, and R. Brandt. 2000. Interaction of tau with the neural membrane cortex is regulated by phosphorylation at sites that are modified in paired helical filaments. *J. Biol. Chem.* 275: 15733–15740.
36. Farah, C. A., S. Perreault, …, N. Leclerc. 2006. Tau interacts with Golgi membranes and mediates their association with microtubules. *Cell Motil. Cytoskeleton.* 63:710–724.
37. Wille, H., G. Drewes, …, E. Mandelkow. 1992. Alzheimer-like paired helical filaments and antiparallel dimers formed from microtubule-associated protein tau in vitro. *J. Cell Biol.* 118:573–584.
38. Crowther, T., M. Goedert, and C. M. Wischik. 1989. The repeat region of microtubule-associated protein tau forms part of the core of the paired helical filament of Alzheimer's disease. *Ann. Med.* 21:127–132.
39. Kajander, T., A. L. Cortajarena, and L. Regan. 2006. Consensus design as a tool for engineering repeat proteins. *Methods Mol. Biol.* 340:151–170.
40. Chen, P. S., T. Y. Toribara, and H. Warner. 1956. Microdetermination of phosphorus. *Anal. Chem.* 28:1756–1758.
41. Fiske, C. H., and Y. Subbarow. 1925. The colorimetric determination of phosphorus. *J. Biol. Chem.* 66:375–400.
42. Kucerka, N., S. Tristram-Nagle, and J. F. Nagle. 2005. Structure of fully hydrated fluid phase lipid bilayers with monounsaturated chains. *J. Membr. Biol.* 208:193–202.
43. Trexler, A. J., and E. Rhoades. 2009. α-Synuclein binds large unilamellar vesicles as an extended helix. *Biochemistry.* 48:2304–2306.
44. Nath, A., A. J. Trexler, …, E. Rhoades. 2010. Single-molecule fluorescence spectroscopy using phospholipid bilayer nanodiscs. *Methods Enzymol.* 472:89–117.
45. Rhoades, E., T. F. Ramlall, …, D. Eliezer. 2006. Quantification of α-synuclein binding to lipid vesicles using fluorescence correlation spectroscopy. *Biophys. J.* 90:4692–4700.
46. Elson, E. L., and D. Magde. 1974. Fluorescence correlation spectroscopy. 1. Conceptual basis and theory. *Biopolymers.* 13:1–27.
47. Friedhoff, P., M. von Bergen, …, E. Mandelkow. 1998. A nucleated assembly mechanism of Alzheimer paired helical filaments. *Proc. Natl. Acad. Sci. USA.* 95:15712–15717.
48. Necula, M., and J. Kuret. 2004. A static laser light scattering assay for surfactant-induced tau fibrillization. *Anal. Biochem.* 333:205–215.
49. Dorn, I. T., K. R. Neumaier, and R. Tampe. 1998. Molecular recognition of histidine-tagged molecules by metal-chelating lipids monitored by fluorescence energy transfer and correlation spectroscopy. *J. Am. Chem. Soc.* 120:2753–2763.
50. Pu, M. M., M. F. Roberts, and A. Gershenson. 2009. Fluorescence correlation spectroscopy of phosphatidylinositol-specific phospholipase C monitors the interplay of substrate and activator lipid binding. *Biochemistry.* 48:6835–6845.
51. Reference deleted in proof.
52. Rusu, L., A. Gambhir, …, J. Rädler. 2004. Fluorescence correlation spectroscopy studies of Peptide and protein binding to phospholipid vesicles. *Biophys. J.* 87:1044–1053.
53. Takakuwa, Y., C. G. Pack, …, M. Kinjo. 1999. Fluorescence correlation spectroscopy analysis of the hydrophobic interactions of protein 4.1 with phosphatidyl serine liposomes. *Biophys. Chem.* 82:149–155.
54. Tsui, F. C., D. M. Ojcius, and W. L. Hubbell. 1986. The intrinsic pKa values for phosphatidylserine and phosphatidylethanolamine in phosphatidylcholine host bilayers. *Biophys. J.* 49:459–468.
55. Jeganathan, S., M. von Bergen, …, E. Mandelkow. 2008. The natively unfolded character of tau and its aggregation to Alzheimer-like paired helical filaments. *Biochemistry.* 47:10526–10539.

56. Yao, T. M., K. Tomoo, …, T. Taniguchi. 2003. Aggregation analysis of the microtubule binding domain in tau protein by spectroscopic methods. *J. Biochem.* 134:91–99.

57. Sibille, N., A. Sillen, …, G. Lippens. 2006. Structural impact of heparin binding to full-length Tau as studied by NMR spectroscopy. *Biochemistry*. 45:12560–12572.

58. Morar, A. S., A. Olteanu, …, G. J. Pielak. 2001. Solvent-induced collapse of alpha-synuclein and acid-denatured cytochrome c. *Protein Sci.* 10:2195–2199.

59. Mylonas, E., A. Hascher, …, D. I. Svergun. 2008. Domain conformation of tau protein studied by solution small-angle X-ray scattering. *Biochemistry*. 47:10345–10353.

60. Galván, M., J. P. David, …, R. Mena. 2001. Sequence of neurofibrillary changes in aging and Alzheimer's disease: a confocal study with phospho-tau antibody, AD2. *J. Alzheimers Dis.* 3:417–425.

61. Gellermann, G. P., T. R. Appel, …, S. Diekmann. 2006. Paired helical filaments contain small amounts of cholesterol, phosphatidylcholine and sphingolipids. *Biol. Chem.* 387:1267–1274.

62. Klein, C., E. M. Kramer, …, J. Trotter. 2002. Process outgrowth of oligodendrocytes is promoted by interaction of fyn kinase with the cytoskeletal protein tau. *J. Neurosci.* 22:698–707.

63. Lee, G., S. T. Newman, …, G. Panchamoorthy. 1998. Tau interacts with src-family non-receptor tyrosine kinases. *J. Cell Sci.* 111:3167–3177.

64. Surridge, C. D., and R. G. Burns. 1994. The difference in the binding of phosphatidylinositol distinguishes MAP2 from MAP2C and Tau. *Biochemistry.* 33:8051–8057.

65. Shea, T. B. 1997. Phospholipids alter tau conformation, phosphorylation, proteolysis, and association with microtubules: implication for tau function under normal and degenerative conditions. *J. Neurosci. Res.* 50:114–122.

66. Alberts, B., D. Bray, …, J. D. Watson. 1994. Molecular Biology of the Cell, 4th ed. Garland Publishing, New York, NY.

67. Wells, K., A. A. Farooqui, …, L. A. Horrocks. 1995. Neural membrane phospholipids in Alzheimer disease. *Neurochem. Res.* 20:1329–1333.